Accepted Manuscript

Interpretation of high resolution aeromagnetic data for Lineaments study and occurrence of Banded Iron Formation in Ogbomoso Area, Southwestern Nigeria

Michael Adeyinka Oladunjoye, Abel Idowu Olayinka, Mustapha Alaba, Moruffdeen Adedapo Adabanija

PII: S1464-343X(15)30089-3

DOI: 10.1016/j.jafrearsci.2015.10.015

Reference: AES 2397

To appear in: *Journal of African Earth Sciences*

Received Date: 9 June 2014

Revised Date: 1 October 2015

Accepted Date: 22 October 2015

Interpretation of high resolution aeromagnetic data for Lineaments study and occurrence of Banded Iron Formation in Ogbomoso Area, Southwestern Nigeria

Michael Adeyinka Oladunjoye [1], Abel Idowu Olayinka[1], Mustapha Alaba[1]
[1]Department of Geology, University of Ibadan, Ibadan, Nigeria (ma.oladunjoye@mail.ui.edu.ng)

Moruffdeen Adedapo Adabanija [2,#]

[2]Department of Earth Sciences, Ladoke Akintola University of Technology, Ogbomoso, Nigeria (maadabanija@lautech.edu.ng; tunde.adabanija@gmail.com; +234-803378-6592)

[#] Correspondence author

Abstract

The quest for solid mineral resource as an alternative for oil income in Nigeria presents opportunity to diversify the resource base of the country. To fill some information gap on the long abandoned Ajase and Gbede Banded Iron Formations (BIF) in Ogbomoso area, Southwestern Nigeria, high resolution aeromagnetic data of Ogbomoso - Sheet 222 was interpreted; to provide a better understanding of the mode of occurrence of the iron ore and associated structural features and geologic model. These were accomplished by subjecting reduced-to-pole (RTP) residual aeromagnetic intensity map to various data filtering and processing involving total horizontal derivative, vertical derivative, Upward Continuation (UC), Downward Continuation (DC), Euler Deconvolution at different Spectral Indices (SI), and Analytical signal using Geosoft Oasis Montaj 6.4.2 (HJ) data processing and analysis software. The resultants maps were overlain, compared and or plotted on RTP residual aeromagnetic intensity map and or geological map and interpreted in relation to the surface geological map.

Positive magnetic anomalies observed on the RTP residual aeromagnetic intensity map ranged from 2.1 to 94.0 nT and associated with contrasting basement rocks, Ajase and Gbede BIF; while negative magnetic anomalies varied between -54.7 nT and -2.8 nT and are associated

with intrusive bodies. Interpreted lineaments obtained from total horizontal derivative map were separated into two categories namely ductile and brittle based on their character vis-à-vis magnetic anomalies on RTP intensity map. Whilst the brittle lineaments were interpreted as fracture or faults; the ductile lineaments were interpreted as folds or representing the internal fabric of the rock units. In addition prominent magnetic faults mainly due to offset of similar magnetic domain/gradient were also interpreted. The iron ore mineralization is distributed within the eastern portion of the study area with Ajase BIF at relatively greater depth (0.5 – 2.0 km) compared to Gbede BIF (0.50 – 0.75 km) and confined probably along a fault lineament or lying conformably on topographic bedrock depression suggesting it is structurally controlled. The accepted Euler deconvolution structural index of 2.0 and 3.0 indicate horizontal cylinder and sphere geological model respectively.

Orientation and mode of occurrence of Ajase BIF have been established. However, coring and a complimentary geophysical prospecting preferably gravity is recommended to deduce and establish the thickness of Ajase BIF in order to estimate the possible tonnage of the deposit.

Keywords: Banded Iron Formation, Magnetic anomalies, Lineaments, High resolution aeromagnetic data, Geological features/model

INTRODUCTION

Contrasts in physical properties of ore minerals, ore-related minerals and the rocks which host them are critical to the successful application of geophysical methods (SEG 1966, 1990; Van Blaricom 1980; Hoover *et al* 1991, 1992). Magnetic method relies on contrast in magnetic susceptibility. It is the oldest and most widely used geophysical exploration tool (Likkason

2014). The effectiveness of the method depends mainly on the presence of magnetite in the rocks of the surveyed area. Other important magnetic minerals are pyrrhotite and hematite (Telford *et al* 1990; Kars *et al* 2014; Guo 2015). A prime goal of magnetic surveys is direct detection of metallic ore bodies through delineation of associated anomalies, which are usually positive and high in magnetic intensity. Other objectives include determination of trends, extents and geometries of magnetic bodies in an area, and to interpret them in terms of geology. Structural trends are faithfully reproduced in magnetic patterns, but assignment of rock type is ambiguous, since ranges of values of magnetic susceptibilities of different rock types may overlap (Damaceno *et al* 2015). Susceptibility may vary considerably, even within the same rock type. In general, sedimentary rocks have the lowest susceptibilities and mafic igneous rocks the highest. High magnetic signature could also be associated with cultural iron contamination and authigenic alterations in sedimentary rocks, possibly caused by hydrocarbon migration (Costanzo-Alvarez *et al*, 2000; Kearey and Brooks, 2002; Aldana *et al*, 2003). Thus, magnetic data (ground or air-borne) has played prominent role in revealing subsurface information especially in geological mapping and mineral prospecting in areas with limited outcrop (Ghazala 1993; Chernicoff *et al* 2002; Porwal *et al* 2006; Allek and Hamoudi 2008; Schetselaar and Ryan 2009).

Several analytical data processing tools or enhancements namely Fourier filtering techniques and others such as power spectra, Euler deconvolution and analytical signal provide value-added products that may contribute to the geological interpretation of magnetic data through better images or maps produced. Fourier filtering techniques involve transformation of data that are broad band in nature e.g potential field data such as gravity and magnetic to Fourier domain using Fast Fourier Transform. In this form the data can be dealt with as a function of wave number or wavelength such that a number of manipulations can be done to enhance and suppress/remove the information of interest and otherwise respectively (Bhattacharya 1966, Spector and Grant 1970). Fourier filtering techniques are broadly divided into geophysical and mathematical filters. Whilst former filters namely upward continuation, downward continuation and vertical derivatives are based on physics of potential field and therefore ideally suited for gravity and magnetic data; mathematical filters e.g. horizontal derivative, high and low pass filters such as Butterworth, Gaussian and simple low-pass/high-pass cut off filters such as anti-alias filters are applicable to any kind of data. In this paper, total horizontal derivative, upward continuation, downward continuation, and Euler deconvolution at different Spectral Indices (SI) have been applied to reduced-to-pole (RTP) residual aeromagnetic intensity map of Ogbomoso. The study was aimed to provide information on the long abandoned Ajase and Gbede Banded Iron Formations (BIF) in Ogbomoso area, Southwestern Nigeria using Geosoft Oasis Montaj 6.4.2 (HJ) software. The specific objectives of study include providing a better understanding of the mode of occurrence of the iron ore in the area, the associated structural features and geologic model. Previous studies using terrestrial magnetic study have shown occurrences of iron bodies at Oko, Gbede and Ajase, in trenches trending 32^{o}, hosted within a ferruginous quartzite that is underlain by banded Gneiss and extend laterally enough to about 303 m (Ancelloni and Maranzana, 1965).

GEOLOGICAL SETTING

The study area is within north of Ogbomoso metropolis, Southwestern Nigeria and covers about 3,025 square km between longitudes 04^{o} 00" 00'E to 04^{o} 30" 00'E and latitudes 08^{o} 00" 00'N to 08^{o} 30" 00'N. Ajase iron ore occurs 19.2 km NE of Ogbomoso and can be easily accessed from Iporin and Gambari on the Ogbomoso-Ilorin road (Figure 1). The area around

Ogbomoso is underlain by the Precambrian Basement Complex rocks. The lithological units are Quartzite, Granite-Gneiss and Banded Gneiss (Figure 2). The quartzite is part of the Migmatite-Gneiss Quartzite Complex, mainly composed of quartz (Eluyemi *et al*, 2012). The Ajase iron-ore deposit lies in an area of gently undulating topography covered by a lateritic cap. Exposures of rock in situ are rare and with the exception of the iron-quartzite and weathered mica schist exposed in the trenches, the only other rock present in the area is gneiss which outcrops on the Iporin-Ogbomoso road, about 3.2 km SW of the trenches. This is in agreement with Ancelloni and Maranzana (1965) report on the geological sequence in boreholes drilled over the Ajase iron-ore deposit as comprising surface lateritic cap covering a weathered mica schist series including bands of iron-quartzite in the middle part, and gneiss at the bottom (Table 1).

MATERIAL AND METHOD

Description of the data

The data set were total field aeromagnetic data (sheet number 222) acquired during high resolution airborne geophysical surveys of Nigeria between 2003 and 2009 by Fugro Airborne Survey Limited for Nigerian Geological Survey Agency (NGSA, 2009). The survey was flown in drape mode using real time differential GPS at a sensor mean terrain clearance of 75m. Traverse and tie line spacing were 500 m and 2000 m respectively while flight and tie line directions were NW-SE and NE-SW respectively (NGSA, 2008). The data were de-cultured, leveled, corrected for International Geomagnetic Reference Field (IGRF), gridded at an appropriate cell size that enhances anomaly details and reduces possible noise and latitude effects (Patterson and Reeves, 1985).

Table 1. Geological sequence obtained from three boreholes drilled in the study area (Ancelloni and Maranzana, 1965)

Borehole GSN No	Depth drilled	Average recovery (%)	Iron-quartzite recovery (%)	Interval	Comments
3081	182’6’’	18.8	90	55’3’’ – 56’0’’	Iron-quartzite (9’’ recovered)
				59’8’’ – 59’10’’	Iron-quartzite (2’’ recovered)
				76’0’’ – 79’0’’	Iron-quartzite (2’7’’ recovered)
				152’7’’ – 152’9’’	Iron-quartzite (2’’ recovered)
3082	168’8’’	15.8	51	108’0’’ – 108’9’’	Iron-quartzite (9’’ recovered)
				118’0’’ – 119’0’’	Iron-quartzite (2½’’ recovered)
				126’7’’ – 128’0’’	Iron-quartzite (8’’ recovered)
3083	153’7’’	3.3	100	80’7’’ – 81’10’’	Iron-quartzite (1’3’’ recovered)
				84’6’’ – 87’0’’	Iron-quartzite (2’6’’ recovered)

Deployment of high resolution aeromagnetic data

The total field data were recorded profile by profile in Excel format and delivered in Oasis montaj^{TM} grid (x,y,z) file format where x is the geographic easting value; y is the geographic northing value; with x and y in Universal Transverse Marcator (UTM) convention as Oasis montaj used in this study utilises the real ground distance in meter; and z magnetic intensity value. The bounding geographic coordinates were converted into degrees using Rockware^{TM} 15 software so that the resultant maps can be compared with geological map of the area for interpretation purpose.

Data Processing

An important goal of data processing especially with 2-dimensional magnetic field data is to simplify the complex information provided in the original data. In this form, improve data quality is achieved for better understanding and constructive geological deductions (Ajakaiye *et al*, 1986; Blakely, 1996; Hinze *et al*, 2005; Nwankwo *et al*, 2011). One such simplification is to derive map(s) on which the amplitude of the displayed function is directly or simply related to a physical property of the underlying rocks as well as inherent structural features and other desired parameters. In this paper, RTP residual aeromagnetic intensity map of the study area was subjected to various data filtering and processing tools involving total horizontal derivative, upward continuation, downward continuation, and Euler Deconvolution at different spectral indices (SI) using Geosoft Oasis Montaj 6.4.2 (HJ) software.

Total horizontal derivatives were applied to delineate boundaries of intrusive bodies (Aryamanesh, 2009; Damaceno *et al* 2015), faults, and other lateral changes using edge detection techniques (Langenheim and Jachens, 2014; Li *et al* 2014). Mathematical and theoretical details of these filters are as discussed by Miller and Singh (1994), Blakely (1996) and Verduzco *et al*

(2004). The Total horizontal derivatives map produced from RTP residual aeromagnetic intensity map (Figure 3) is as depicted in Figure 4. The lineaments extracted from the derivative map and their orientations representations on Rose diagram are as shown in Figure 5. The azimuthal distribution of the extracted lineaments and the associated orogeny is as on Table 2.

Table 2. Distribution and orientations of the lineaments and the associated orogeny

Lineaments	Trends	Orogeny
88%	Northeast – Southwest	Pan African
7%	Northwest - Southeast	Kibaran
5%	East-west	Liberian

Euler deconvolution was applied to determine the depth to the basement of the magnetic anomalies. The Euler deconvolution method relates the vertical and horizontal gradient of the residual magnetic intensity values with help of geometry of the magnetic bodies given by the structural index (e.g. Thompson, 1982; Barbosa *et al.*, 1999). Solutions obtained from Euler deconvolution are also useful in delineation of source geometry and boundaries. It could also be used for fault mapping if the proper structural index (SI) value is used. For a homogeneous point source N = 3, a linear source (line of dipoles or poles, and for a homogeneous cylinder, rod, etc.) N = 2, for intrusive bodies (thin layer, dike, etc.) N = 1, for a contact, vertex of a block and a pyramid with a big height N = 0 (Table 3). Hence in this paper, SI values of 0, 1, 2, 3 have been used and the values of SI at which matches in relation to the geologically realistic results obtained were accepted as solution. The depth obtained from Euler deconvolution was compared with average depth (Z) to sources obtained from radially averaged power spectrum plot (Salem and Ali, 2014). The Euler deconvolution depth plot obtained from RTP residual aeromagnetic intensity map is as shown in Figure 6 while its corresponding radially average power spectrum is as in Figure 7.

Continuation processes comprising upward and downward were employed to discriminate against shallow and deeper magnetic sources respectively. Its operation allows the transformation of data measured on one surface to some higher surface (Nabighian *et al*, 2005) and tends to smooth the original data by attenuating short wavelength or high frequency anomalies relative to their long wavelength or low frequency counterparts (upward continuation) or vice versa (Feumoe *et al* 2012; Langenheim and Jachens, 2014). The processed output map reveals the remaining low or high frequency anomalies indicating corresponding deeper or shallow sources in the bedrock depending on the level of continuation. In this study, the magnetic amplitude maps obtained from RTP residual aeromagnetic intensity map at various levels of upward and downward continuation are as shown in Figure 8. The RTP aeromagnetic residual magnetic intensity map and other output maps obtained from processing and filtering as compared to or superimposed on geologic map (e.g. Bultman 2015) of the area were interpreted.

INTERPRETATIONS AND DISCUSSION OF RESULTS

Reduced-to-pole aeromagnetic intensity map

The colour shaded RTP aeromagnetic intensity map of the area shown in Figure 3 indicates anomalies A, B, C, D, E, F, G, H, I, J and K as positive magnetic anomalies ranging from 2.1 to 94.0 nT characterized the central, northeastern, northwestern, southeastern and eastern parts; whilst anomalies L, M and N are negative magnetic anomalies ranging between -

Table 3: Structural indices for various geological models (Adapted from: Amigun *et al*, 2012b; Olasehinde *et al*, 2012; Yaghoobian *et al*, 2009; GETECH, 2007 and Reid *et al*, 1990)

Geological Model	**Number of Infinite Dimensions**	**Structural Index (SI)**
Sphere	0	3
Pipe	1 (Z)	2
Horizontal cylinder	1 (X or Y)	2
Dyke	2 (Z and X or Y)	1
Sill	2 (X and Y)	1
Contact	3 (X, Y and Z)	0

54.7 nT and -2.8 nT characterize the southern, southwestern and north central part of the map. Careful examination of RTP aeromagnetic intensity map with the geological map of the area (Figure 2) suggests the negative anomalies are associated with granitic intrusion (Mume 1964; Mcenroe *et al* 2004; Adabanija *et al* 2013; Biyiha-Kelaba *et al* 2013). This is as exemplified by intrusion of quartzitic schist by porphyritic biotite-hornblende granite/migmatite granite gneiss and fine-grained biotite granite at the southern and north central part respectively. On the other hand; areas of positive magnetic anomalies are associated with various lithologic units such as migmatite, granite gneiss, biotite-hornblende-gneiss, porphyritic biotite-hornblende granite and fine grained biotite granite. Both Ajase and Gbede BIF are also located within areas of positive magnetic anomalies with Gbede BIF at higher magnetic anomaly (58.4 – 94 nT) compared to Ajase BIF (49.4 – 58.4 nT).

Depth to basement estimate

The results of Euler solutions obtained are as shown in Figure 6 for SI value of 0 (Figure 6a), 1.0 (Figure 6b), 2.0 (Figure 6c), and 3.0 (Figure 6d). At SI=0 (Figure 6a); there are no tightest clustering along any geologic structure or magnetic anomalies suggesting SI of value zero is not a solution and hence rejected (Thompson 1982; Reid *et al.* 1990; Feumoe *et al* 2012). However, the Euler solutions of SI value of 1.0, 2.0 and 3.0 appear good match as there are clusters around some notable anomalies Ajase and Gbede BIF at the eastern part (Figure 6b, 6c); and along synform and antiform-like feature in Figure 6d. From Figure 6b, the depth to basement around Ajase BIF ranged between 250 m and greater than 1000 m; while Gbede BIF is relatively at shallower depth 250 m to 750 m. Whereas in Figure 6c, the depth to basement of clusters around Gbede BIF and Ajase BIF ranged from 500 m to 750 m and 500 m to greater than 1000 m respectively. Likewise in Figure 6d; the cluster over Gbede and Ajase BIF as well as the synform and antiform-like feature indicated depth range of 750 m to greater than 1000 m. Thus Euler deconvolution at structural index value of 1, 2 and 3 are possible depth solutions corresponding to sill/dyke, horizontal cylinder and sphere geological model (Table 3).

The calculated spectral analysis and radially average power spectrum plot of the study area is as depicted in Figure 7. The depth curve in Figure 7a has three tangential straight line segments which slope decreases with increasing frequency. The first segment (red line) has the greatest descent (about -34.146) while the second (green line) and third segments (blue line) has gradient of about -5.106 and -2.326 respectively. The peaks within the first segment (Figure 7b) with greatest descent give the depth estimate of deepest source, whilst the peaks within the least gradient (Figure 7b) give the depth estimate of the shallowest source. These correspond to 1 – 3.8 km and 0.5 – 1.8 km (Figure 7b) and correlate with results of Euler deconvolution specifically at SI of 2.0 and 3.0. Hence the structural index of 2.0 and 3.0 are most acceptable indicating horizontal cylinder and sphere geological model.

Basement mapping

The RTP residual AMI map obtained from the continuation process is as shown in Figure 8. Relatively high positive magnetic anomalies T and S ranging from 0.319 nT to 0.405 nT in the northwestern part of Figure 8a are visible at an upward continuation distance of 1000 m and retained the same magnitude with increase in upward continuation to 4000 m corresponding to depth of 500 m and 2000 m respectively. This is based on rule of thumb, the data depth-continued at a height of z corresponds to the depth of z/2 (Paananen 2013). However, some areas experienced sharp changes from high amplitude anomaly to low amplitude anomaly delineated by black curve and oval in Figure 8a at the south-southwestern, central, north central, eastern, southeastern, north-northwestern and northeastern part. Such areas are fault zones (Parasnis, 1986; Fierberg, 2002; and Amigun *et al* 2012a, 2012b). Gbede BIF is on the fault zone at the eastern part as exemplified by its amplitude which decreased from 0.144 - 0.164 nT (red and yellow colour) to 0.002 – (-0.024) nT (blue and green colour) at upward continuation of 1000 m (Figure 8a) and 4000 m (Figure 8b) respectively. However, the amplitude range observed over Ajase BIF was unchanged. This suggests Gbede BIF is at relatively shallow magnetic source compared to Ajase BIF at depth range of 0.5 km to 2.0 km. Thus the differential magnetic intensity value over Gbede BIF (58.4 – 94 nT) and Ajase BIF (49.4 – 58.4 nT) observed on RTP map (Figure 3) could be attributed to their different depth of occurrence.

Structural Framework

Normalized magnetic derivatives are well suitable for structural mapping (e.g. Verduzco *et al* 2004; Fairhead and Williams 2006; Fairhead *et al* 2007; Salem *et al* 2008). It is on this premise that the total horizontal derivative map (Figure 4) has been interpreted to deduce prominence geological structures in the current study. For this purpose, the lineaments extracted from total horizontal derivative map (Figure 5a) were overlain on RTP magnetic intensity map (Figure 3) using Arc-GIS 10.3 software and are geologically characterized as either ductile when their features are concordant with magnetic anomalies or brittle when their features cross cut the magnetic anomalies (Paananen 2013). Based thereon, the areas enclosed in white oval (Figure 9) indicate ductile deformation zones and are mostly east-west lineaments; whilst the remaining areas mostly dominated by NE-SW and NW-SE lineaments are brittle deformation zone and as such could exhibit structural features such as faults and fractures. This is as corroborated by magnetic faults map (Figure 10) obtained from superimposition of the magnetic lineaments extracted from the total horizontal derivative map on the geological map using Arc-GIS 10.3 software. The magnetic faults are faults mainly due to offset of similar magnetic domains/gradients (Gay, 1972; Gunn *et al* 1997; and Paananen 2013). These faults are in white and black colour (Figure 10) and at different orientations: WWS-EEN, SSW-NNE, NW-SE and NNW-SSE. These faults are interpreted as sinistral (white colour) and dextral (black). The sinistral faults showing clockwise rotation indicate the emplacement of quartz-schist prior to deformation that led to the formation of sinistral fault as observed at the southern part of the study area. These sinistral faults must have formed contemporaneously with open isoclinal fold (F1) through D1 with a schistocity S1 which axial plane AP (blue colour, Figure 10) trends east-west. Some of the dextral faults act as conduits for emplacement of elongated granitic intrusions as exemplified by tadpole-like porphyroblastic gneiss and fine-grained biotite granite at the southern and north central part of the area respectively. Generally, the pattern and configuration of the faults (sinistral and dextral) suggests block rotation in the area.

Consequently; the orientations of some of the basement lithology in the area could also be deduced from the map in Figure 10. This is attributed to the fact that Total horizontal derivative are amongst other data enhancing tools e.g. analytic signal, upward continuation and tilt derivative that are particularly valuable in amplifying orientations of magnetic sources which in turn could be tectonically controlled (Paananen 2013). This is as exemplified by concordance of some of the lineaments especially the NE-SW with the strike of fine-grained biotite granite, porphyroblastic gneiss and migmatite granite gneiss.

The lineaments distribution as observed in Figure 9 indicates rarity of magnetic lineaments at the eastern part as corroborated by Total horizontal derivative gray scale map

(Figure 4b) suggests the deformation that has taken place in the area was probably accompanied by a topographic bedrock depression filled by soil. This must have probably resulted to slight decrease in the measured magnetic field as exemplified by difference in magnetic anomaly of Gbede BIF (58.4 – 94 nT) and Ajase BIF (49.4 – 58.4 nT) further establishing Ajase BIF at a relatively deep depth compared to Gbede BIF.

The structural styles are as indicated by Rose diagram in Figure 5b namely E-W, NW-SE and NE-SW with NW-SE as most dominance (Table 2) constituting 88% of the 80 extracted lineaments. The oldest orogeny recorded for the Precambrian basement complex of Nigeria is Liberian > 2500 ma and is characterized by E-W lineaments (D1). The Pan African thermotectonic event Ca 650 ma ± 150 ma is characterized by NE-SW and NW-SE lineaments (D3) (Odeyemi, 1988). The lineaments traces therefore suggest relict imprints of Liberian orogeny localized in the North-western part of the study area underlain by migmatite gneiss. In close association with these relict imprints are the predominant NE-SW lineaments set which occur conformably with granitic intrusions (Figure 2) and therefore suggest Pan African origin. The Pan African orogeny (650 ± 150 ma) witnessed the emplacement of granitoid bodies which introduced heat into the country rock. This occurrence may cause curvilinear lineament indicating F1. A trace of curvilinear lineament is as observed at the bottom centre of the study area (Figure 9). Furthermore, the rarity of lineaments as well as its sparse distribution at the eastern and northwestern end section of the area (Figure 9) respectively may mean that the area is deep seated and has witnessed some sort of subsidence thereby creating a basin for deposition of sediments believed to be Eburnean 2200 ± 100 ma (Birrimean supra crustal) (Rahaman *et al* 1981).

CONCLUSIONS

An attempt has been made on the interpretation of the aeromagnetic data of Ogbomoso - Sheet 222 using Geosoft Oasis Montaj 6.4.2 (HJ) data processing and analysis software. From the results of interpretation, the distribution of the concealed BIF at Ajase and Gbede, depths to magnetic sources, basement structures, boundaries and lithologic contacts in Ogbomoso area were established. Positive and negative magnetic anomalies observed on the reduced-to-pole residual aeromagnetic intensity map ranged from 2.1 to 94.0 nT and -54.7 nT to -2.8 nT respectively. While the positive anomalies are associated with contrasting basement rocks, Ajase and Gbede BIF; the negative anomalies are associated with intrusive bodies. The lineaments obtained from the total horizontal derivative map indicated fractures, faults and folds geological features. The varied orientations of the geologic features and structural styles suggest the study area has undergone more than one tectonic event.

The iron ore mineralization is distributed within the eastern portion of the study area with Ajase BIF at relatively greater depth about 0.5 – 2.0 km compared to Gbede BIF about 0.50 – 0.75 km. The Ajase BIF is probably on a deep seated fault or lying conformably on topographic bedrock depression suggesting it is structurally controlled. The accepted Euler deconvolution structural index of 2.0 and 3.0 indicate horizontal cylinder and sphere geological model respectively.

The mode of occurrence and associated geologic features of Ajase BIF has been deduced from the analysis and interpretation of aeromagnetic data of Ogbomoso Sheet 222. However, coring and a complimentary geophysical prospecting preferably gravity is recommended to deduce and establish the thickness of Ajase BIF that is required to calculate the possible tonnage of the formation.

AKNOWLEDGEMENT

The authors acknowledge comments, critical and thoughtful reviews of the anonymous reviewers which have greatly enhanced the quality of the paper. Our immense gratitude to our colleague, Olukayode A. Afolabi Structural geology/Geochemistry research team lead, Department of Earth Sciences, Ladoke Akintola University of Technology Ogbomoso Nigeria for useful and incisive discussion on structural styles and other geologic interpretations.

REFERENCES

Adabanija, M. A., Olasehinde, P. I., Ologunaye, B. T. and Ojetunde, L. A., 2013. Investigation of subsurface geologic features of Oke-Alapata Area, Ogbomoso, South-western Nigeria. Journal of Environment and Earth Science 3(14): 119-151.

Bultman, M.W., 2015. Detailed interpretation of aeromagnetic data from the Patagonia Mountains area, southeastern Arizona: U.S. Geological Survey Scientific Investigations Report 2015-5029, 25 p

Ajakaiye, D.E., Hall, D.H., Miller, T.W, Verherjen, P.J.T., Awad, M.B. and Ojo, S.B.1986. Aeromagnetic anomalies and tectonic trends in and around the Benue Trough Nigeria. Nature, 319: 582-584.

Aldana, M., Costanzo-Alvarez, V. and Diaz, M. 2003. Magnetic and mineralogical studies to characterize oil reservoirs in Venezuela. The Leading Edge, 22(6): 526.

Allek, K and Hamoudi M. 2008. Regional-scale aeromagnetic survey of the south-west of Algeria: A tool for area selection for diamond exploration. Journal of African Earth Sciences, 50: 67-78

Amigun, J. O., Afolabi, O. and Ako, B. D. 2012a. Application of Airborne Magnetic Data to Mineral Exploration in the Okene Iron Ore Province of Nigeria. International Research Journal of Geology and Mining (IRJGM), 2(6): 132-140.

Amigun, J. O., Afolabi, O. and Ako, B. D. 2012b. Euler 3-D Deconvolution of Analytic Signal of Magnetic Anomalies over Iron Ore Deposit in Okene, Nigeria. Journal of Emerging Trends in Engineering and Applied Sciences (JETEAS), 3(4): 711-717.

Ancelloni, G. and Maranzana, M. 1965. Final Report on the Iron-Ore Ajase, near Ogbomoso, Ibadan Province. Geological Survey Nigeria Report No. 1444

Aryamanesh, M. 2009. Aeromagnetic data interpretation to locate buried faults in Yazd Province- Iran. World Applied Science Journal, 6(10): 1429-1432.

Barbosa, V.C.F., Silva, J. B. C. and Medeiros, W. E. 1999. Stability analysis and improvement of structural index estimation in Euler deconvolution. Geophysics, 64: 48-60

Bhattacharyya, B. K. 1966. Continuous spectrum of the total magnetic field anomaly due to a rectangular prismatic body. Geophysiscs, 31:97-121

Biyiha-Kelaba, W., Ndougsa-Mbarga, T., Yene-Atangana, J. Q., Ngoumou, P. C. and Tabod, T. C., 2013. 2.5D Models Derived from the Magnetic Anomalies Obtained by Upwards Continuation in the Mimbi Area, Southern Cameroon. Journal of Earth Sciences and Geotechnical Engineering, 3(4): 175-199

Blakely, R. J., 1996. Potential theory in gravity and magnetic applications. Cambridge University Press.

Chernicoff, C. J., Richards, J. P. and Zappettini, E. O. 2002. Crustal lineament control on magmatism and mineralization in northwestern Argentina: Geological, geophysical and remote sensing evidence. Ore geology reviews, 21(3-4): 127-155

Costanzo-Alvarez, V., Aldana, M., Aristeguieta, O., Marcano, M. C. and Aconcha, E. 2000. Study of magnetic contrasts in the Guafita oil field (South-western Venezuela). Physics and Chemistry of the Earth, Part A: Solid Earth and Geodesy, 25(5): 437- 445.

Damaceno, J. G., de Castro, D. L. and Mocitaiba, L. S. R. 2015. Geophysical study of volcanic bodies, Potiguar basin (RN): preliminary results. 14th International congress of the Brazillian Geophysical Society Rio de Janeiro Brazil August 3-6 2015: 1-4

Eluyemi, A. A., Olorunfemi, M. O. and Ogunfolakan, M. A. 2012. Integrated Geophysical Investigation of Orile-Oje Archaeological site, Ogbomosho, Southwest Nigeria. The Pacific Journal of Science and Technology, 13(1): 615-628.

Fairhead, J.D. and Williams, S.E., 2006. Evaluating Normalized Magnetic Derivatives for Structural Mapping. SEG 2006 New Orleans Extended Abstract.

Fairhead, D., Williams, S. and Ben Salem, A., 2007. Structural Mapping from High Resolution Aeromagnetic Data in Namibia using Normalized Derivatives. EGM 2007 International Workshop: Innovation in EM, Grav and Mag Methods: a new Perspective for Exploration. Capri, Italy, April 15 – 18, 2007

Feumoe, A. N. S., Ndougsa-Mbarga, T., Manguelle-Dicoum, E. and Fairhead, J. D. 2012. Delineation of tectonic lineaments using aeromagnetic data for the south-east Cameroon area. Geofizika, 29(2): 175-192

GETECH. 2007. Advanced Processing and Interpretation of Gravity and Magnetic Data. GETECH Plc., Kitson House Elmete Hall Leeds, UK. 27pp.

Ghazala, H. H., 1993. Geological and structural interpretation of air borne surveys and its significance for mineralization, southeastern desert Egypt. Journal of African Earth Sciences (and the Middle East), 16(3): 273-285

Guo, W. W., 2015. Magnetic mineralogical characteristics of Hamersley iron ores in Western Australia. Journal of Applied Mathematics and Physics, 3: 150-155

Hinze, J., Aiken, C., Brozena, J., Coakley, B., Dater, D., Flanagan, G., Forsberg, R., Hildenbrand, T., Keller, G. R., Kellogg, J., Kucks, R., Li, X., Mainville, A., Morin, R., Pilkington, M., Plouff, D., Ravat, D., Roman, D., Urrutia-Fucugauchi, J., V´eronneau, M., Webring, M. and Winester, D. 2005. New standards for reducing gravity data: The North American gravity database. Geophysics, 70(4): 25–32.

Hoover, D.B., Grauch, V.J.S., Pitkin, J.A., Krohn, D., and Pierce, H.A., 1991, Getchell trend airborne geophysics-an integrated airborne geophysical study along the Getchell trend of gold deposits, North-Central Nevada. In: Raines, G.L., Lisk, R.E., Schafer, R.W., and Wilkinson, W.H., (eds)., Geology and Ore Deposits of the Great Basin, Geological Society of Nevada, 2:739-758.

Hoover, D.B., Heran, W.D., and Hill, P.L., eds., 1992, The geophysical expression of selected mineral deposit models: U.S. Geological Survey Open-file Report 92-557, 129 p.

Kars, M., Aubourg, C., Labaume, P., Berquo, T. S. and Cavailhes, T. 2014. Burial diagenesis of magnetic minerals: new insights from the Grés d'Annot Transect SE France. Minerals, 4:667-689

Kearey, P. and Brooks, M., 2002. An Introduction to Geophysical Exploration. 3rd Edition. Blackwell Science Publication.

Langenheim, V.E., and Jachens, R.C., 2014, Aeromagnetic data, processing, and maps of Fort Irwin and vicinity, California, chap. I *of* Buesch, D.C., ed., Geology and geophysics applied to groundwater hydrology at Fort Irwin, California: U.S. Geological Survey Open-File Report 2013–1024

Li, L., Han, L., and Huang, D. 2014. Normalized edge detection and the horizontal extent and depth of geophysical anomalies. Applied Geophysics, 11(2): 149-157

Likkason, O. T. 2014. Exploring and using the magnetic methods. In: Advance geoscience remote sensing. In-Tech: 141-174

McEnroe, S. A., Skilbrei, J. R., Robinson, P., Heidelbach, F., Langenhorst, F. and Brown, L. L. 2004. Magnetic anomalies, layered intrusions and Mars, Geophys. Res. Lett., 31, L19601

Miller, H.G. and Singh, V., 1994. Potential field tilt- A new concept for location of potential field sources. Journal of Applied Geophysics, 32: 213-217.

Mume W. G., 1964. Negative total-intensity magnetic anomalies in the southeast of south Australia. Journal of Geophysical Research, 69(2):309-315

Nabighian, M. N. and Hansen, R. O. 2005. Unification of Euler and Werner deconvolution in three dimensions via the generalized Hilbert transform. Geophysics, 66: 13-21.

Nigerian Geological Survey Agency, 2008. Airborne geophysical survey total magnetic intensity map of Ogbomoso (Sheet 222) area.

Nigerian Geological Survey Agency, 2009. Geological map of Ogbomoso (Sheet 222) area.

Nwankwo, L. I., Olasehinde, P. I. and Akoshile, C. O., 2011. Heat flow anomalies from the spectral analysis of airborne magnetic data of Nupe Basin, Nigeria. Asian Journal of Earth Sciences, 4(1): 20-28.

Odeyemi, I. B. 1988. Lithostratigraphy and Structural Relationships of the Upper Precambrian Metasediments Igarra area, Southwestern Nigeria. In: Precambrian Geology of Nigeria, (eds) P. O. Oluyide, W. C. Mbonu, A. E. Ogezi, I. G. Egbiniwe, A. C. Ajibade and A. C. Umeji. Geol. Surv. of Nigeria. 111 - 125.

Olasehinde, A., Ashano, E. C. and Singh, G. P. 2012. Structural analysis of the Ropp Complex, north central Nigeria, using magnetic anomaly and landsat ETM imagery. Continental J. Earth Sciences, 7(1): 1 – 8.

Paananen M, 2013. Completed lineament interpretation of the Olkiluoto region. Posiva 2013-02 ISBN 978-951-652-234-3

Parasnis, D. S., 1986. Principles of Applied Geophysics. Chapman Hall, London, pp. 43-44.

Patterson, N. R. and Reeves, C. V., 1985. Effects of the equatorial electroject on aeromagnetic data acquisition. Journals of International Geophysics, 65(2): 55.

Porwal, A., Carranza, E. J. M. and Hale, M. 2006. Tectonostratigraphy and base-metal mineralization controls, Aravalli province (Western India): New interpretations from geophysical data analysis. Ore geology reviews, 29(3-4): 287-306

Rahaman, M. A., Tubosun, I. A. and Ocan, O. O., 1981. Preliminary U-Pb ages on Charnockitic rocks from Akure-Ado Ekiti area. Abstr. 22nd Annual Conference of the Science Association of Nigeria, Jos

Reid, A.B., Allsop, J.M., Granser, H., Millett, A.J. and Somerton, I.W. 1990. Magnetic interpretation in three dimensions using Euler deconvolution. Geophysics, 55: 80-91.

Salem, A., Williams, S., Fairhead, D., Smith, R. and Dhananjay, R., 2008. Interpretation of magnetic data using tilt-angle derivatives. Geophysics, Vol.73, p. L1 – L10.

Salem, A. and Ali, M. 2014. Mapping basement structures in the northwestern offshore of Abu Dhabi from high resolution aeromagnetic data. Extended abstract, 76th EAGE conference & Exhibition, EarthDoc

Schetselaar, E. M. and Ryan, J. J. 2009. Remote predictive mapping of the Boothia mainland area, Nunavut, Canada: an iterative approach using landsat ETM, aeromagnetic and geological field data. Canadian Journal of Remote Sensing, 35: S72-S94

Society of Exploration Geophysicists 1966, (1967), Mining Geophysics, v. 1, Case Histories; v. 2, Theory: Tulsa, Society of Exploration Geophysicists, 492 p. (v. 1); 708 p., (v. 2).

Society of Exploration Geophysicists 1990, Geotechnical and environmental geophysics, v. 1, Review and Tutorial; v. 2, Environmental and Groundwater, *in* Ward, S.H., ed., Tulsa, Society of Exploration Geophysicists, 389 p., (v. 1); 343 p., (v.2).

Spector, A., and Grant, F. 1970. Statistical models for interpreting aeromagnetic data. Geophysics, 35: 293-302.

Thompson, D. 1982. EULDPH: A new technique for making computer-assisted depth estimates from magnetic data. Geophysics, 47: 31-37.

Telford, W.M, Geldart, L.P, Sheriff, R.E, and Keys, D.A., 1990. Applied Geophysics, Cambridge University Press, Camridge

Van Blaricom, R. 1980. Practical geophysics: Northwest Mining Association, 303 p

Verduzco, B., Fairhead, J. D., Green, C. M. and MacKenzie, C., 2004. New insights into magnetic derivatives for structural mapping. The Leading Edge, 23: 116-119.

Yaghoobian, A., Boustead, G. A. and Dobush, T. M., 2009. Object delineation using Euler's Homogeneity Equation. Proceedings of SAGEEP '92, San Diego, California.

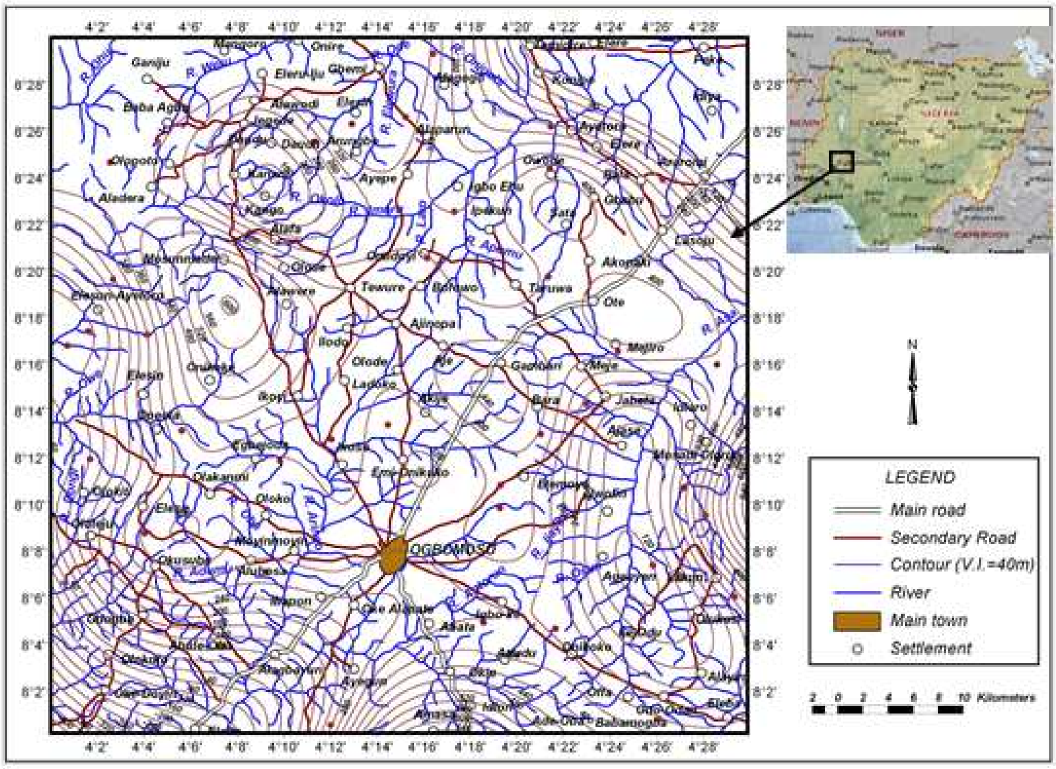

Figure 1: Location and accessibility map of Ogbomoso area (Google Earth Satellite Imaging, 2007)

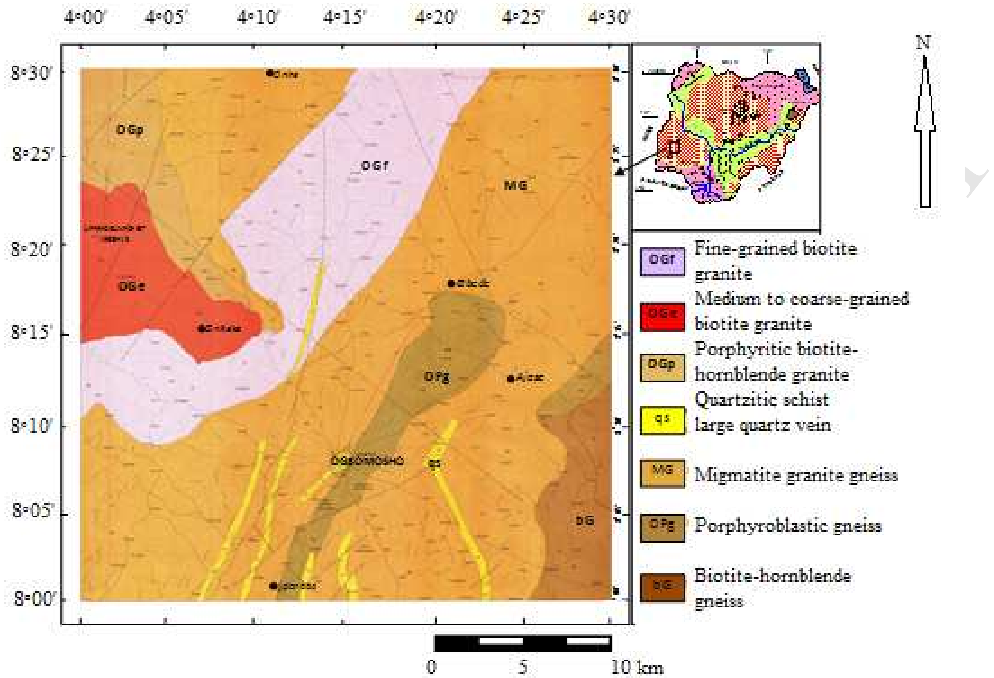

Figure 2. Geological map of the study area (NGSA, 2009)

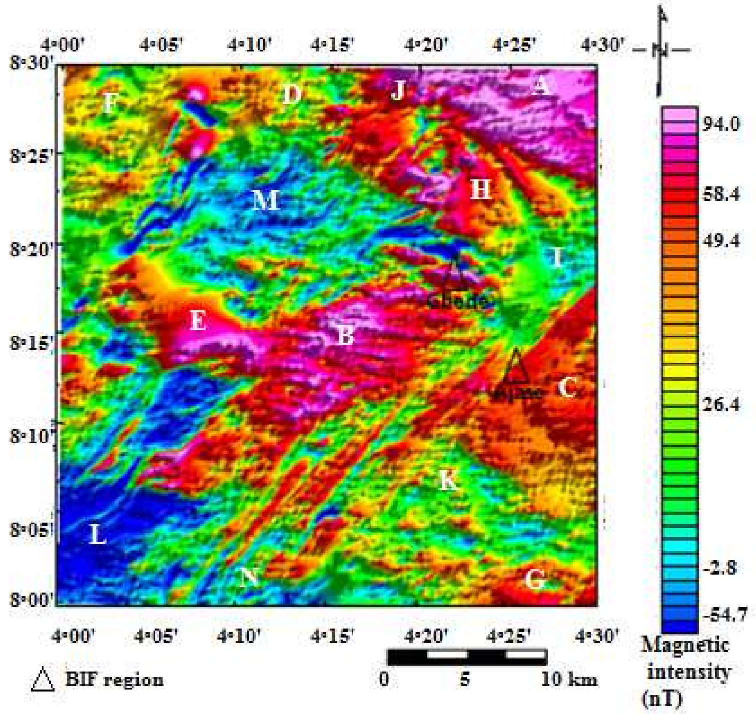

Figure 3. Colour shaded reduced-to-pole (RTP) residual aeromagnetic intensity map showing magnetic anomalies

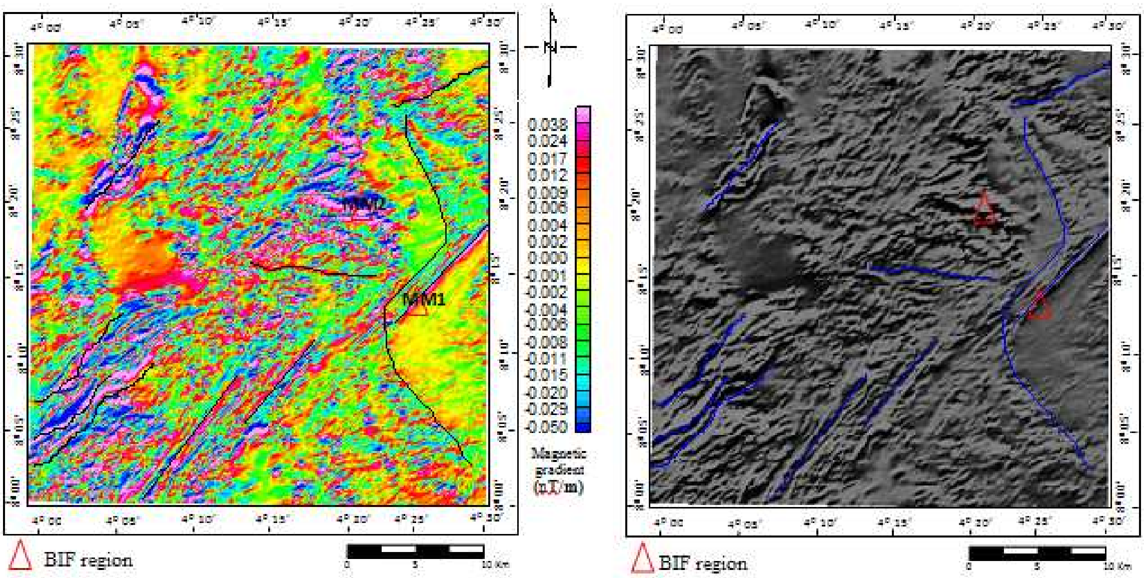

(a) (b)

Figure 4. Total horizontal derivative of reduced-to-pole aeromagnetic intensity map (a) Colour shaded map; (b) Grey shaded map.

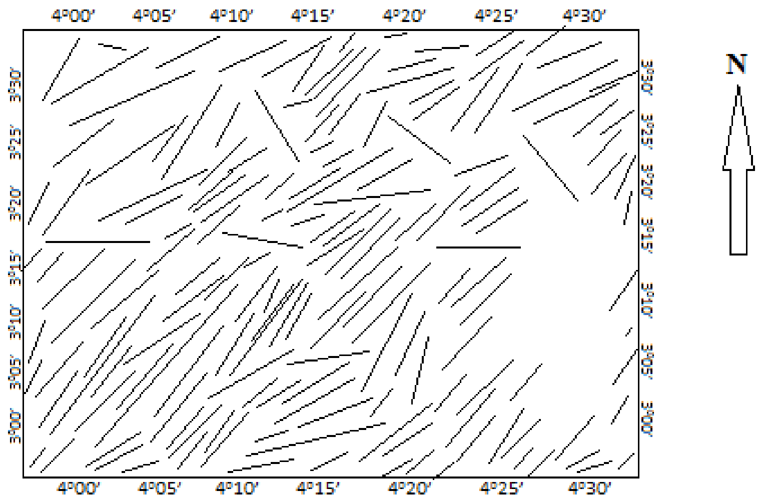

(a)

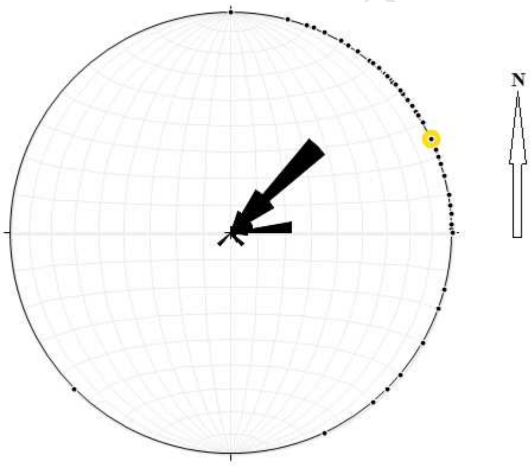

(b)

Figure 5. (a) Some lineaments extracted from the total horizontal derivative map; (b) Rose diagram showing orientations of the lineaments

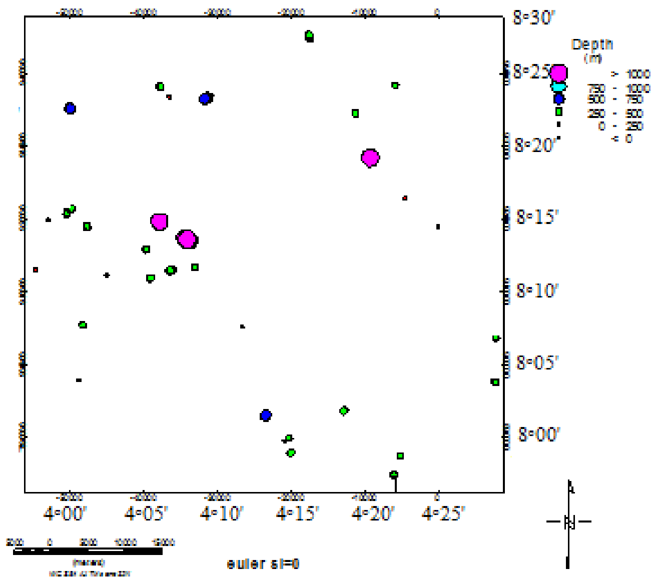
8°30′
8°25′
8°20′
8°15′
8°10′
8°05′
8°00′
4°00′
4°05′
4°10′
4°15′
4°20′
4°25′
Depth (m)
> 1000
750 - 1000
500 - 750
250 - 500
0 - 250
< 0
euler si=0

(a)

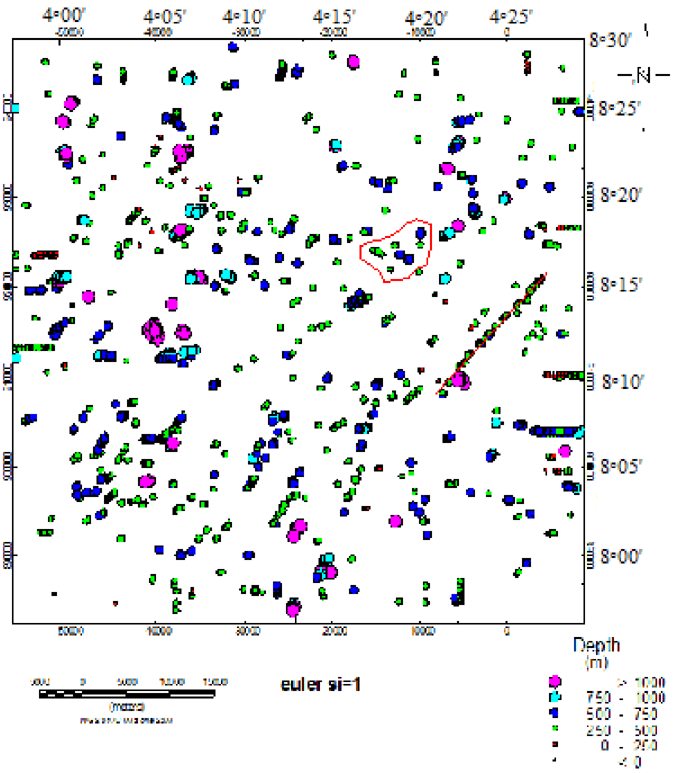
4°00′
4°05′
4°10′
4°15′
4°20′
4°25′
8°30′
8°25′
8°20′
8°15′
8°10′
8°05′
8°00′
euler si=1
Depth (m)
> 1000
750 - 1000
500 - 750
250 - 500
0 - 250
< 0

(b)

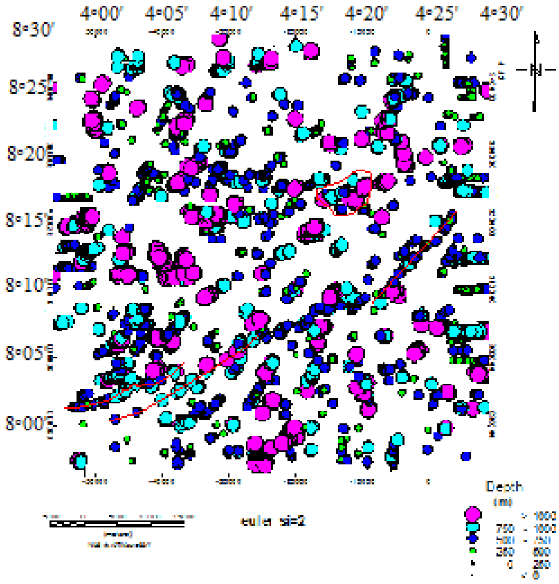

(c)

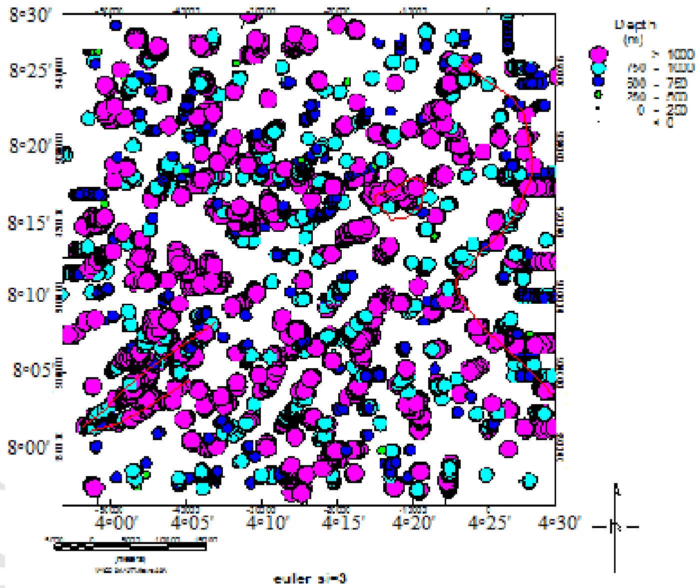

(d)

Figure 6. Euler deconvolution depth plot at different Structural Index (SI) obtained from RTP residual aeromagnetic intensity map (a) SI = 0, (b) SI = 1, (c) SI = 2, (d) SI = 3

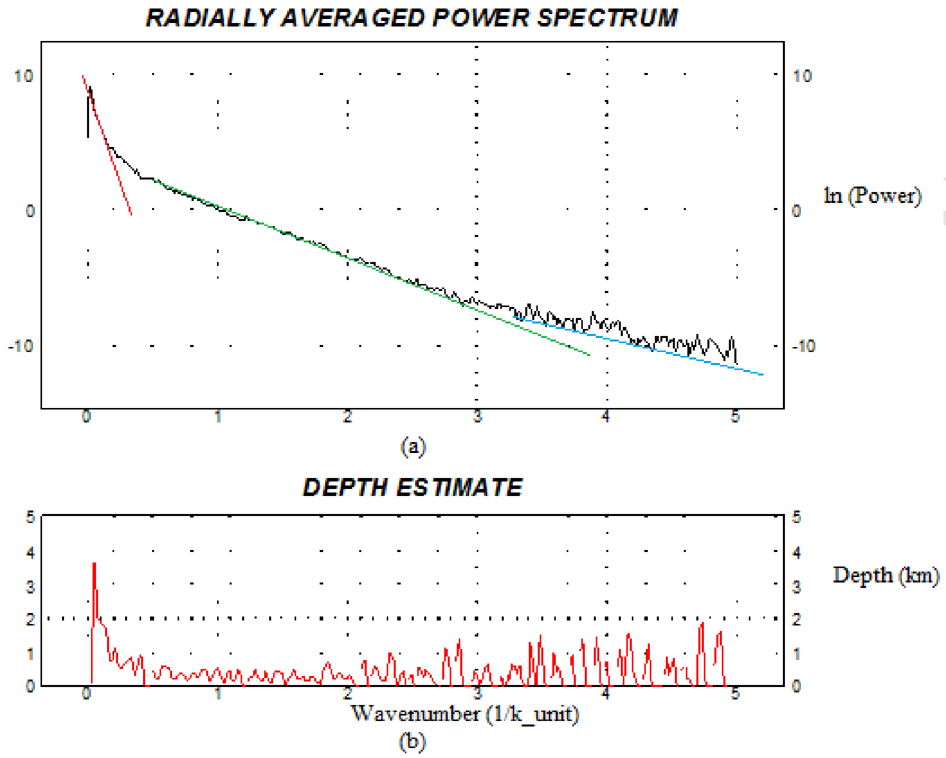

Figure 7. Spectral analysis and radially average power spectrum plot of the study area. (a) Radially averaged power spectrum; (b) Depth estimate

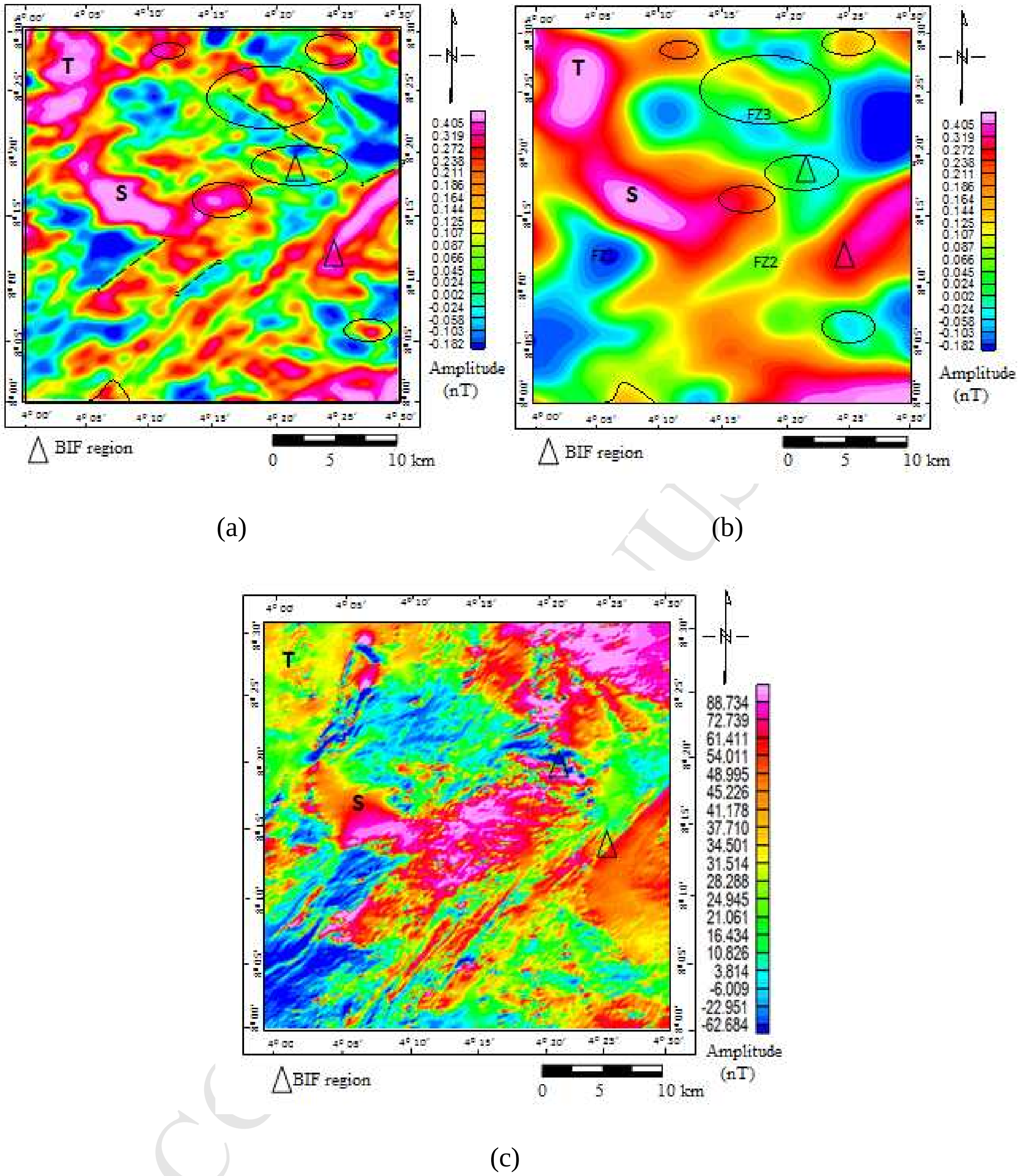

Figure 8. Magnetic amplitude map obtained from RTP residual aeromagnetic intensity map after (a) upward continuation to 1000m, (b) upward continuation to 4000m, (c) downward continuation to 100m

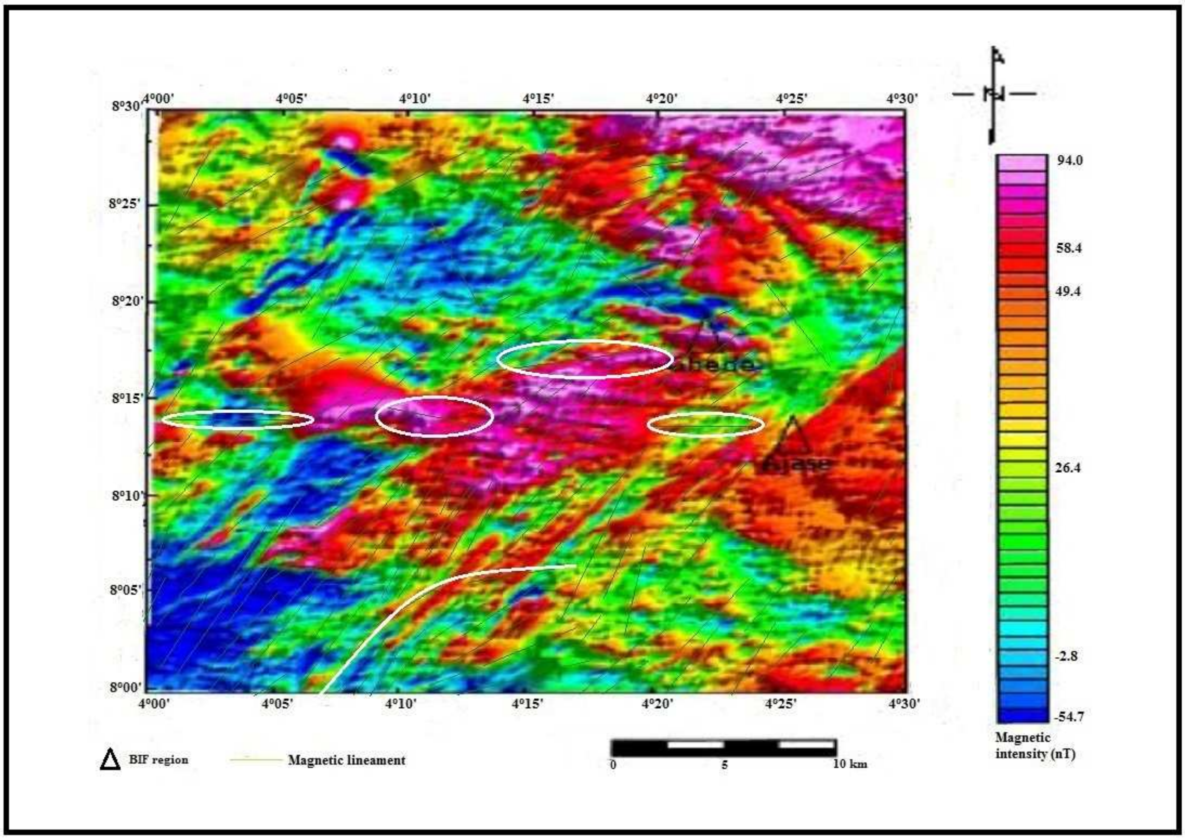

Figure 9. Magnetic lineaments classification map

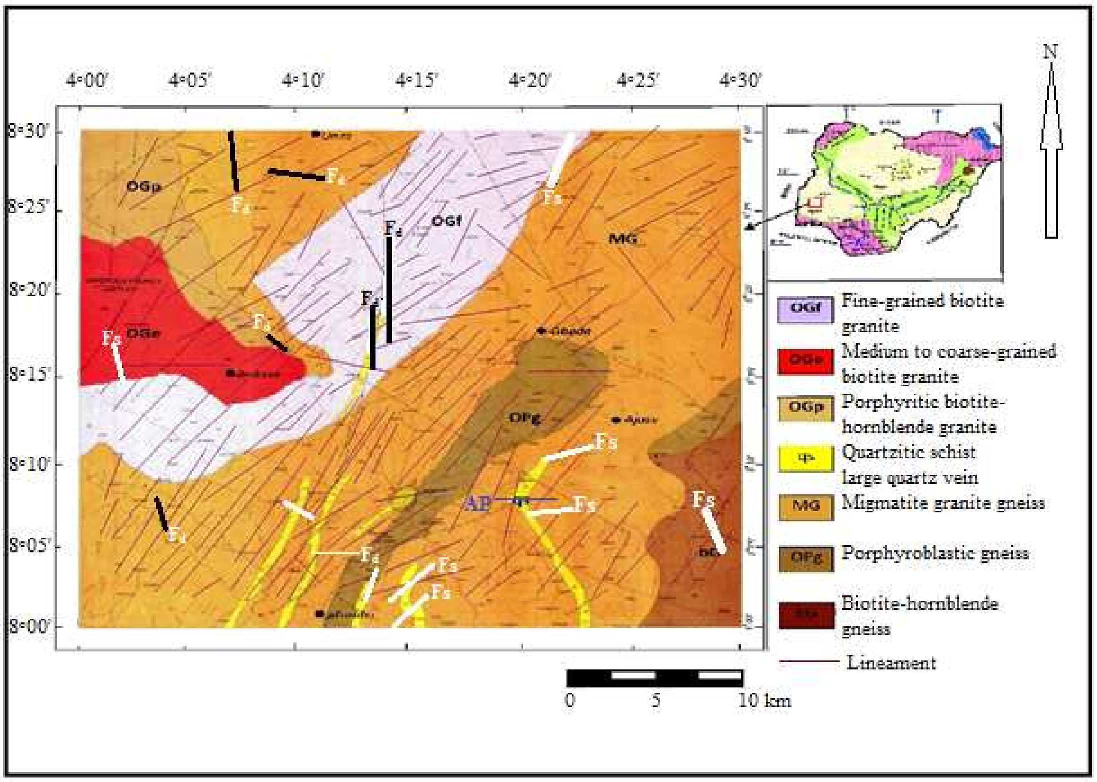

Figure 10. Faults map

- Analytical data processing techniques were applied to reduced-to-pole residual aeromagnetic intensity map.

- Magnetic data filtering and processing results were plotted on geological map of the area.

- Magnetic anomalies are associated with contrasting basement rocks, Ajase and Gbede Banded Iron Formation (BIF), and intrusive bodies.

- Mode of occurrence of the BIF was established.

- Varied orientations of the geologic features suggest the study area has undergone more than tectonic event.